Ambient seismic noise imaging of a tailings dam internal structure

AUTHORS:
Thulisile Kunjwa[1,2]
Moctar Doucouré[1]

AFFILIATIONS:
[1]Africa Earth Observatory Network (AEON), Nelson Mandela University, Gqeberha, South Africa
[2]Department of Geosciences, Nelson Mandela University, Gqeberha, South Africa

CORRESPONDENCE TO:
Thulisile Kunjwa

EMAIL:
kunjwat@gmail.com

DATES:
Received: 23 June 2023
Revised: 27 Mar. 2024
Accepted: 19 June 2024
Published: 04 Dec. 2024

HOW TO CITE:
Kunjwa T, Doucouré M. Ambient seismic noise imaging of a tailings dam internal structure. S Afr J Sci. 2024;120(11/12), Art. #16366. https://doi.org/10.17159/sajs.2024/16366

ARTICLE INCLUDES:
☒ Peer review
☐ Supplementary material

DATA AVAILABILITY:
☐ Open data set
☐ All data included
☒ On request from author(s)
☐ Not available
☐ Not applicable

EDITORS:
Michael Inggs
Thywill Dzogbewu

KEYWORDS:
tailings, seismic interferometry, ambient seismic noise, Green's function, imaging

FUNDING:
South African National Research Foundation

Several tailings dam failures have been reported over the past few decades, raising questions about the stability of these structures. Over the past 30 years, there have been more severe failures of tailings dams, which have resulted in damage to the environment, fatalities and severe socio-economic issues. It is often impossible to predict when tailings dams could fail, so there is an urgent need to develop cost-effective methods for monitoring their stability and preventing such catastrophic events. Recent advancements in techniques related to ambient seismic noise have the potential to introduce new approaches to subsurface imaging and monitoring. In this study, we investigated the potential of using ambient seismic noise to monitor the interior wall of a tailings dam. We used 20 3C short-period geophones to record ambient noise over 3 days continuously. We set up the geophones at the Harmony Gold Mine tailings dam in Welkom, South Africa, along a survey profile approximately 100 m long. Seismic interferometry was used from the recorded data to retrieve empirical Green's functions. We computed the dispersion curves' inversion to determine the dam wall's shear wave velocity at different depths. The calculated shear wave velocity cross-sections revealed a region of reduced velocity within the dam wall, situated between 2 m and 10 m beneath the surface. This zone of low velocity can be a sign of water-saturated material or other subsurface anomalies, which might jeopardise the dam's structure.

Significance:

Tailings dams have a long history of ruptures and collapse. The results from this study indicate that passive seismic interferometry can be a cost-effective tool for imaging and identifying minor changes within the interior of the tailings dam wall. This technique could prove valuable in detecting potential instabilities before they reach a critical stage. This can allow for early intervention and remedial measures, such as reinforcing the dam wall or adjusting the water levels in the tailings dam.

Introduction

Tailings dams store waste after separating ore and gangue in mining operations. Some dams reach dozens of metres in height and stretch over several kilometres.[1] These structures can fail, resulting in catastrophic environmental and social consequences. When a tailings dam collapses, it can release millions of tons of toxic waste into surrounding ecosystems, contaminating water sources, and damaging infrastructure. Estimating the exact number of tailings dams worldwide is challenging, as many operate without regulation or documentation. An estimated 3500 large dams exist worldwide; a significant portion are dedicated to supporting mining operations and can potentially be classified as tailings dams.[2]

South Africa has the highest number of environmentally hazardous tailings dams globally due to the predominance of upstream tailings dams, which are considered unsafe and are banned in some countries.[3] There are over 212 reported tailings dams in South Africa[4], and there have been serious dam failures recorded over the past three decades.

On 22 February 1994, the Merriespruit tailings dam collapsed, resulting in the discharge of 600 000 m^3 of tailings and 90 000 m^3 of tailings water that spilled into the town of Merriespruit. This incident is considered as the most infamous tailings dam accident in South Africa. After a few hours of heavy rain, the dam overtopped and broke, resulting in static liquefaction and the flow slide of a section of the embankment as soon as sufficient toe material had eroded. The disaster resulted in the death of 17 people and the destruction of thousands of houses. Figure 1A and 1B shows an aerial view of the dam after it collapsed and images of the town to which the tailings flowed.

On 24 December 2021, coal mining effluent poured from a collapsed dam at the Zululand Anthracite Colliery (ZAC) mine, causing another tailings dam to break. At least 1 500 000 L of contaminated mining waste flowed close to residences before reaching the Black Umfolozi River, which flows through subsistence farming areas and the Hluhluwe-iMfolozi Game Reserve, where the community depends on the river for drinking water and for watering their crops. Figure 1C and 1D shows areas contaminated by the toxic and acidic coal mine waste released into the rivers that flowed through rural villages, the Hluhluwe-iMfolozi and iSimangaliso nature reserves, and other nearby locations.

The most recent dam failure happened at Jagersfontein in South Africa on 11 September 2022 – most of the tailings discharged from the south of the dam, where there was a breach. The width of the plume reached up to 1.5 km and extended about 8.5 km. The sludge contaminated the Prosesspruit River and several other streams. Many other irrigation and drinking water systems were also polluted.

As investigators commence the collection of post-failure evidence for analysing the breach, initial observations point to overtopping as the underlying cause of the failure.[7] Besides destroying over 50 homes, disrupting water supplies and crops, and displacing nearly 400 people, the disaster resulted in the tragic loss of one human life and approximately 900 farm animals owned by at least 25 farmers.[8]

Establishing and maintaining effective monitoring systems for tailings dams is a complex challenge influenced by technical intricacies, site-specific issues, cost constraints, human errors and data management difficulties.[5] Despite

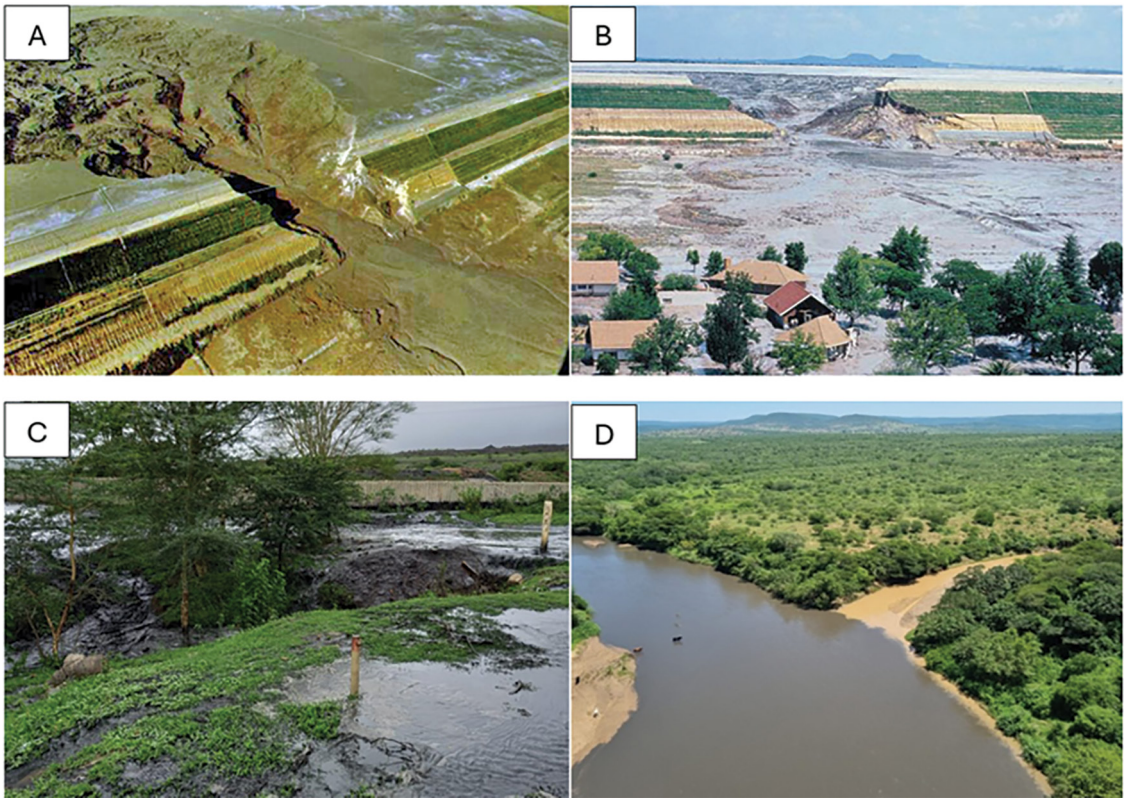

Sources: (A,B): Minerals Council of South Africa[5]; (C) Daily Maverick[6]; (D) Dennis Kelly[6]; reproduced with permission.

Figure 1: (A) An aerial view of the Merriespruit tailings dam after it collapsed; (B) images of the town covered by the sludge; (C) the extent of pollution of the Black Umfolozi River; (D) toxic coal mining waste flowing through Hluhluwe-iMfolozi Game Reserve.

the increasing awareness of potential risks linked to tailings dams, there are significant areas for improvement in detecting and monitoring failures. Monitoring systems often need to be more adequately designed and maintained, and the absence of standardised monitoring guidelines results in inadequate safety measures. Moreover, mining companies rarely share information about their monitoring systems, hindering their effectiveness of evaluation.[9] Communities downstream of these dams are often unaware of the associated risks due to a lack of transparency regarding tailings dam safety.

To address these gaps, increasing investments in monitoring and establishing a transparent reporting system is imperative for accurately assessing and managing these risks. The tailings dam failures observed globally have raised serious questions concerning how government and mining companies deal with the long-term repercussions of 150 years of industrial mining. This study illustrates the potential of using passive seismic interferometry as a tool to image dam walls.

Passive seismic interferometry is a geophysical technique used to estimate properties of the subsurface through the analysis of ambient seismic noise cross-correlation. Alternative approaches to seismic interferometry, such as cross coherence and deconvolution interferometry, are also utilised to derive valuable information about the subsurface environment.[10] This technique has proven to be useful in various applications, including seismic imaging[11], tracking and monitoring groundwater levels[12,13] and exploration of hydrocarbon reservoirs[14]. This technique aims to retrieve the empirical Green's function of the subsurface by using naturally occurring seismic waves generated by various factors, including wind, ocean waves and human activities.

The empirical Green's function serves as an estimate of the Green's function, revealing how a medium, like the Earth's subsurface, responds to a localised energy source. In the field of seismology, the empirical Green's function proves to be a valuable tool, providing essential insights into the acoustic and elastic characteristics of the subsurface.[15,16]

Several studies have successfully demonstrated the possibility of recovering surface waves using seismic interferometry.[15-17] Examining the Earth's subsurface structure encompasses the analysis of surface waves across diverse time intervals. Typically, research in this field has primarily utilised waves with frequencies significantly below 1 Hz to investigate the properties of the crust and upper mantle. However, recent progress in seismic interferometry has broadened the possibilities by extending exploration to frequencies beyond 1 Hz. This advancement has introduced novel opportunities for investigating the subsurface, especially in the range spanning tens to hundreds of meters. Consequently, there is a noticeable trend towards focusing on shorter periods, reflecting an increased interest in studying and understanding the Earth's structure at relatively shallow depths in scientific investigations.[11,18]

Calculating dispersion curves is important in the fields of seismology and geophysics, as they provide crucial insights into the relationship between the seismic wave velocity and frequency. These curves illustrate the variations in the velocity of seismic waves across different frequencies, thereby providing valuable information about the structure of the Earth's subsurface. This approach plays a pivotal role in enhancing our capability to interpret the intricate and dynamic characteristics of the Earth's subsurface. It is also crucial for assessing dam wall stability, especially in locating the phreatic surface and determining soil saturation.[17] Rayleigh waves, generated by P and SV waves interacting with a free surface, have opposite responses to saturation, affecting velocity measurements. Love waves, which are generated when SH waves interact with free surfaces, demonstrate a distinctive decrease in velocity with saturation. This characteristic is the reason why Love waves were chosen for analysis in this study.

Data acquisition

We deployed a total of 20 three-component 14 Hz seismic sensors, each equipped with a sealed gel battery and connected to a three-channel seismic data cube. The synchronisation of time between stations was accomplished using internal GPS modules, and the signal was recorded at a rate of 400 samples per second.

These sensors were positioned along a 95-m survey line, maintaining an interstation spacing of 5 m. To safeguard against adverse environmental conditions, potential animal interference and the risk of contact corrosion from water and soil chemicals, both the data cube and the battery were placed in a sealed plastic box and buried. The sensors were installed to align with north, with their horizontal components oriented east-west in relation to north depicted on the map. The sensors were specifically buried on the tailings dam wall, approximately 1.5 m from the foot of the dam wall. The portion of the dam where the sensors were placed represents only a minor segment of the entire tailings dam at a single elevation. Figure 2A provides an aerial view of the tailings dam where we positioned the stations, while Figure 2B illustrates the distribution of the seismic stations. We planted these stations between cone penetration tests conducted on the tailings dam and above a seepage area at the dam's base.

In this project, we follow the processing scheme outlined by Bensen et al.[18] for data processing of a single station. The procedure consists of three main phases: (1) preparation of data from a single station, (2) cross-correlation calculation and temporal stacking and (3) generation of dispersion curves and inversion of ground profiles. For this project, we developed a MATLAB code for the first two phases of the data processing procedure.

Data processing

The ambient seismic noise recordings or data acquired from the stations require pre-processing before immediate use, as the coherent broadband ambient noise needs to be accentuated prior to cross-correlation.

Ambient seismic noise, known as microseisms, emerges in the 2- to 20-second period range due to standing waves in the ocean, serving as a valuable source of information about oceanic processes. Microseisms generated in lakes, observed within the 0.5- to 2-second period range, share potential generation mechanisms with single- and double-frequency microseisms. This information aids in expanding our understanding of seismic phenomena in lacustrine environments.[19] Additionally, microtremors, characterised by shorter periods, typically less than 1 second, are linked to human activities. The frequencies observed in both microseisms and microtremors encompass the frequency band of body and surface waves, providing a holistic view of natural and human-induced seismic influences.[20,21]

Spectrograms function as visual representations that depict the distribution of frequencies throughout the entirety of a recording. Essentially, they offer a comprehensive overview of the frequency composition present in the recorded signal. Particularly noteworthy in this context is the recognition of distinct and prominent peaks surpassing the 50 Hz threshold, as depicted in Figure 3. These high peaks are

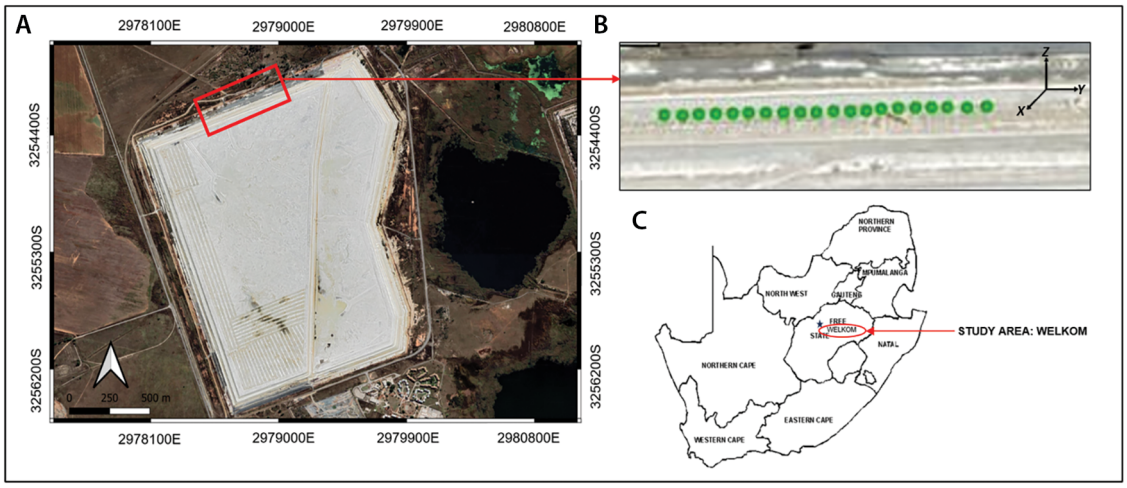

Source: Google Earth (created using the free and open source QGIS).

Figure 2: (A) Aerial view of the tailings dam where the seismic stations were planted; (B) a zoomed in picture of Figure 2A showing the distribution of the seismic stations on the tailings dam; (C) outline map of South Africa, the red area indicates the Free State province where Welkom is located.

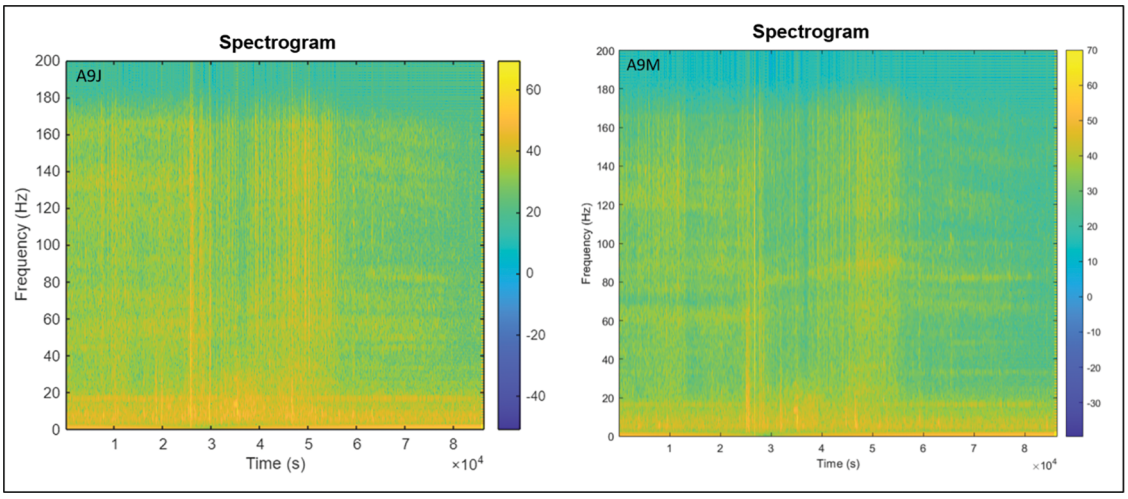

Figure 3: Spectrogram of stations A9J and A9M.

specifically linked to anthropogenic effects, signifying the occurrence of human-generated activities or disturbances within the recorded data.

The spectrogram illustrates temporal variations over time. High frequencies are predominantly observed between 3 and 6 hours, aligning with the commencement of mining operations at the processing plant of the dam being investigated. The heightened frequency during this period is likely associated with human activities. After calculating the spectrograms, the data underwent band-pass filtering to remove high frequencies above 50 Hz before normalisation was applied.

We segmented the data into 10-minute intervals to provide a more detailed view of the signal (Figure 4). This step is crucial for achieving a precise analysis of events and spikes that might not be readily apparent in the original signal.

Temporal normalisation in the time domain assumes significant importance during the preparation of a single station. This reduces the influence of correlated earthquake signals, instrument irregularities and non-stationary noise sources close to the stations.

In this study, we implemented the water-level normalisation method, as explained by Bensen et al.[18] Water-level normalisation is a method commonly used in ambient noise tomography to account for variations in noise levels across different stations or time periods. This normalisation technique involves dividing the seismic data by an estimate of the noise level to achieve a more consistent representation of the ambient noise field. This technique enhances the reliability of seismic data by reducing the influence of non-seismic factors, such as environmental conditions or instrument characteristics, thereby improving the quality of seismic analyses and interpretations.

We applied spectral whitening on the data in the final step of this data processing phase. Ambient noise spectra typically show non-uniformity in the frequency domain, requiring the application of whitening to flatten the spectrum. This step aims to increase the bandwidth of ambient noise while reducing the impact of persistent, spatially isolated noise sources on the signals.

The spectral whitening process involves creating a MATLAB function called 'Whitening'. This function generates a flat Fourier spectrum for a given signal initially exhibiting non-uniformity across a range of frequencies within a defined frequency band. This process includes applying a Hann window to the signal, followed by Fourier transformation, magnitude normalisation and inverse Fourier transformation. Figure 5 illustrates the amplitude spectra of the waveform before whitening, displaying non-uniformity with multiple peaks of varying amplitudes.

Phase 2 of the data processing begins with computation of cross-correlation between all station pairs to obtain empirical Green's functions. The correlation is computed across all components, including north-north, northeast-east, east-east and east-north. Cross-correlation was performed on 10-minute segments between all pairs of sensors. Following computation, the cross-correlations were stacked by summation of the sensor pairs. In this stack, each trace represents the cumulative sum of correlation pairs derived from various sensor pairs.

This summative approach enhances the signal-to-noise ratio and highlights coherent features present in the ambient noise field. The correlation functions pertaining to the vertical component depict estimations of Raleigh waves traversing between sensors, while those of the horizontal transverse signify Love waves. As previously mentioned, the investigation of Love waves is deemed more suitable in this setting. Figure 6 illustrates each trace represents the sum of all the correlation pairs plotted as a function of interstations distance. The cross-correlations are two-sided time functions, encompassing positive and negative time coordinates representing waveforms travelling in opposite directions between stations.

We computed and stored cross-correlation functions for lag times spanning from −2 to 2 seconds. This calculation was determined considering the maximum interstation distance of 95 m (distinct from 85 m) and the slowest anticipated surface wave velocity, and the determined time-series length for the cross-correlation functions is 1.52 seconds. Despite the deployment of 20 stations in the field, it is noted that data from two stations were deemed inadequate for analysis, potentially due to cessation of recording during field operations. Consequently, the data were omitted from the processing and analysis conducted in this study.

The correlation functions of the Love waves show arrival fronts for both positive and negative lag times, related to the velocity of surface wave propagation, and this corresponds to the propagation velocity of the surface waves.

The cross-correlation functions show significant asymmetry in amplitude and spectral content. The observed asymmetry indicates variations between the source and the distance from the source in the radial directions extending outward from the stations.

After completing the computation of daily cross-correlations and the stacking process, we measured phase speeds as functions of the period using the resulting waveform data. The primary objective of this step is to analyse how the velocity of the Love waves changes as a function of frequency.

To calculate the dispersion curves, we employed a phase delay and stack method. In order to create a spatial map of shear wave velocity, consecutive sensors are grouped, and the average dispersion curve for the group is calculated by phase delaying and stacking the correlation functions for each trial velocity at a given frequency. Then, we filtered each stacked correlation function within frequency bands ranging from

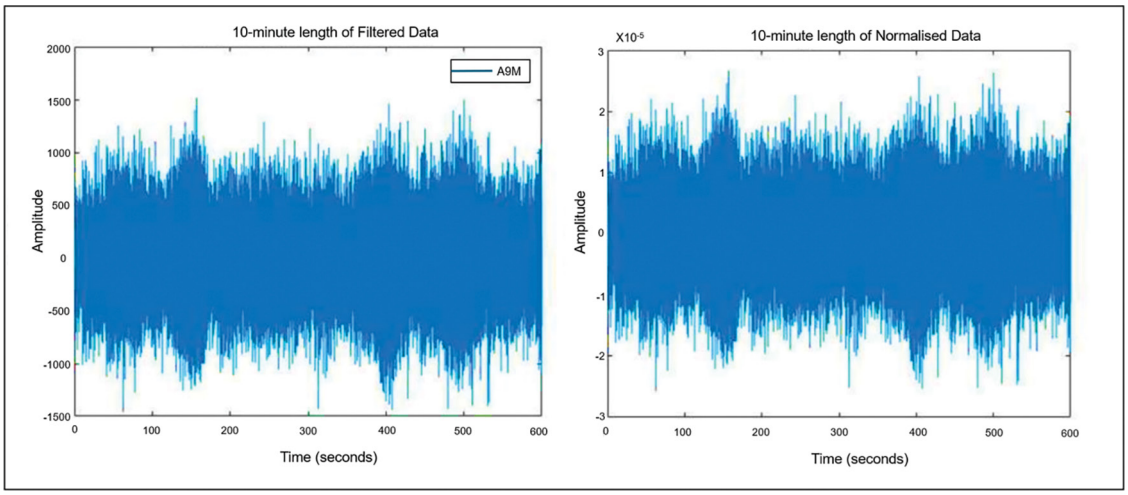

Figure 4: (left) Data that were filtered before being normalised for time using the running absolute mean technique; (right) filtered data after temporal normalisation.

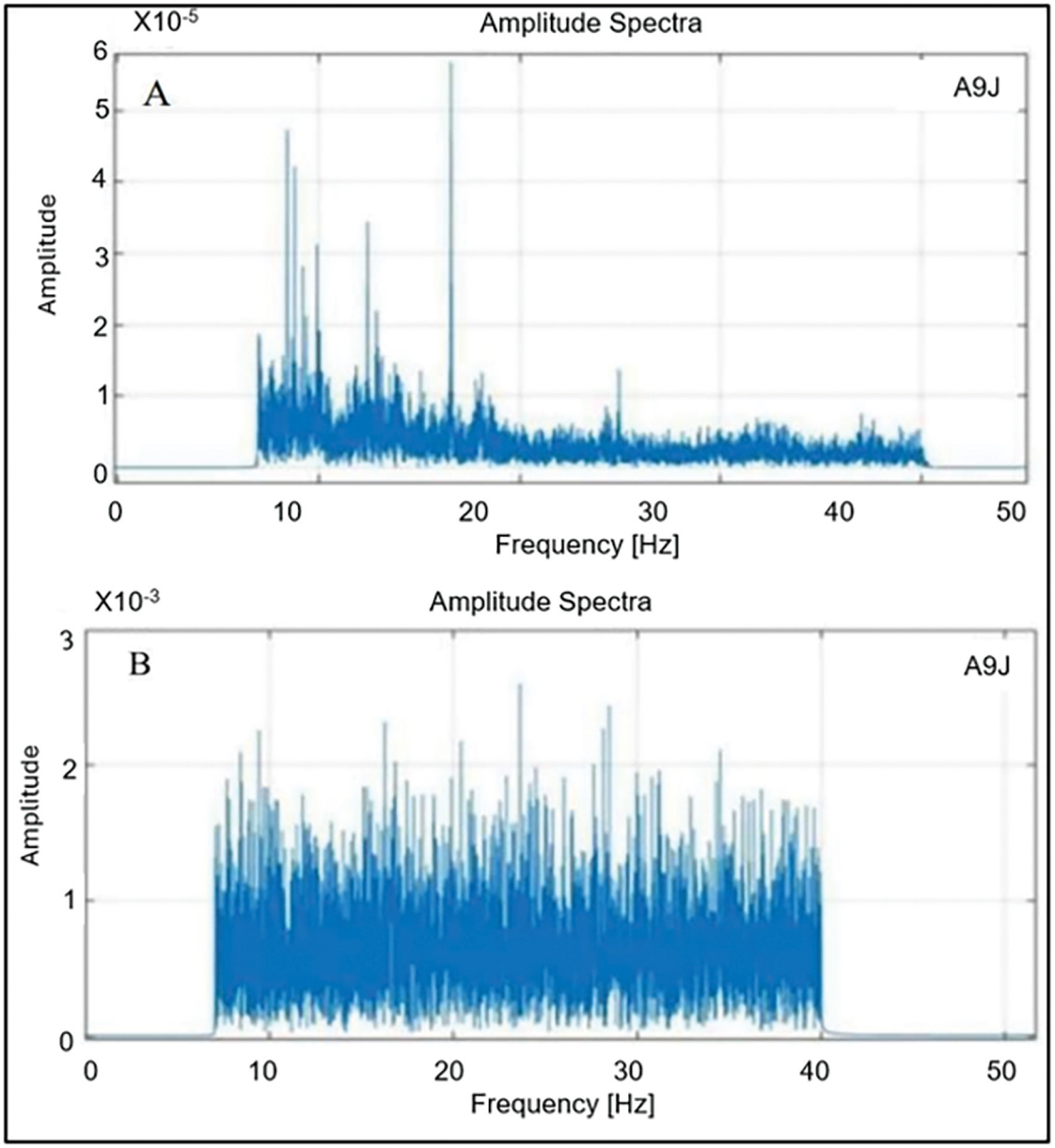

Figure 5: (A) An example of the amplitude spectrum of station A9J before spectral whitening and (B) amplitude spectrum after spectral whitening is applied.

7 Hz to 14 Hz and identified the strongest arrival time for each frequency. Since we knew the distances between the seismic stations, we derived the phase velocity by dividing the distance between the sensors by the selected arrival time. We stacked the curves on each other for multiple pairs of sensors to enhance the signal-to-noise ratio. Figure 7 illustrates the resulting dispersion curves for these sensor pairs.

We calculated average dispersion curves for various velocities at specific frequencies by grouping sensor pairs. The resulting curves consistently demonstrated a common trend, with lower frequencies exhibiting a high velocity range of 138–160 m/s. Some curves displayed relatively high velocities between 10 Hz and 15 Hz, but at frequencies exceeding 20 Hz, certain curves showed a decrease in relative velocity. Anomalous peaks observed in dispersion curves with velocities exceeding 160 m/s may be attributed to the non-uniformity of the ambient noise sources. Variations in the spatial distribution or characteristics of these noise sources within the study area can give rise to localised peaks in dispersion curves.

According to Ivanov et al.[22], surface waves are responsible for approximately 70% of total seismic energy. They are characterised by dispersion, meaning that the different wavelengths have different penetration depths and travel at different velocities. The density and elasticity of the medium influences the speed at which these waves propagate. Longer-period waves are more sensitive to greater depths and penetrate deeper into the Earth's surface and also travel faster generally, as noted by Lin et al.[23]

Surface waves propagate in multiple modes, each with a dispersion curve representing a different velocity range. Higher modes emerge with velocity ranges greater than those of the fundamental mode, with the lowest velocity range. When surface waves propagate through layered horizontal media, they do so multimodally. Different modes of vibration appear at frequencies higher than a specific cut-off frequency. Each mode has its unique propagation velocity, consistently increasing from the fundamental to the higher modes.

In heterogeneous media, higher modes of surface waves emerge due to the constructive interference waves undergoing multiple reflections at layer interfaces.[24] However, detecting these modes is challenging because the energy carried by different overtones is not uniform. The energy distribution depends on frequency, causing a mode to dominate in one frequency band while negligible in another.[24]

We used a wave field transformation procedure explained by Luo et al.[25] to image the various modes and transform the multi-channel record, thereby identifying the dispersion curves based on their altered energy distribution.

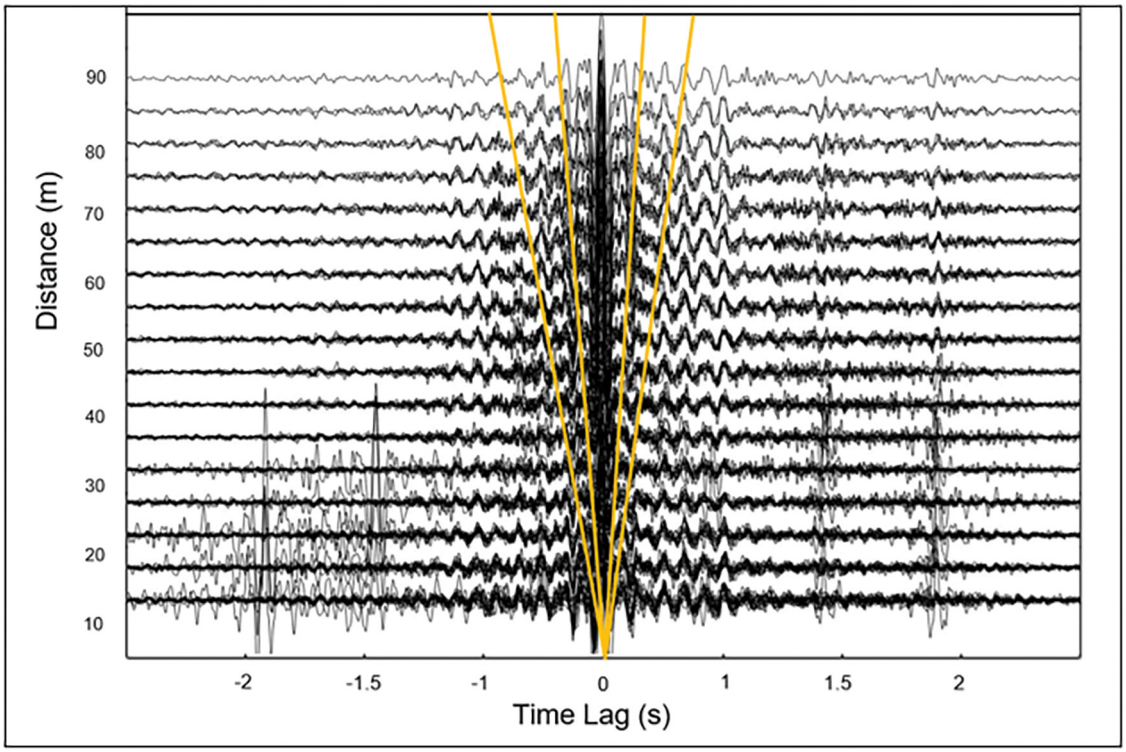

Figure 6: The filtered and normalised data were cross-correlated. The cross-correlation functions are shown against the interstation distance. Both positive and negative lag periods show distinct arrival fronts.

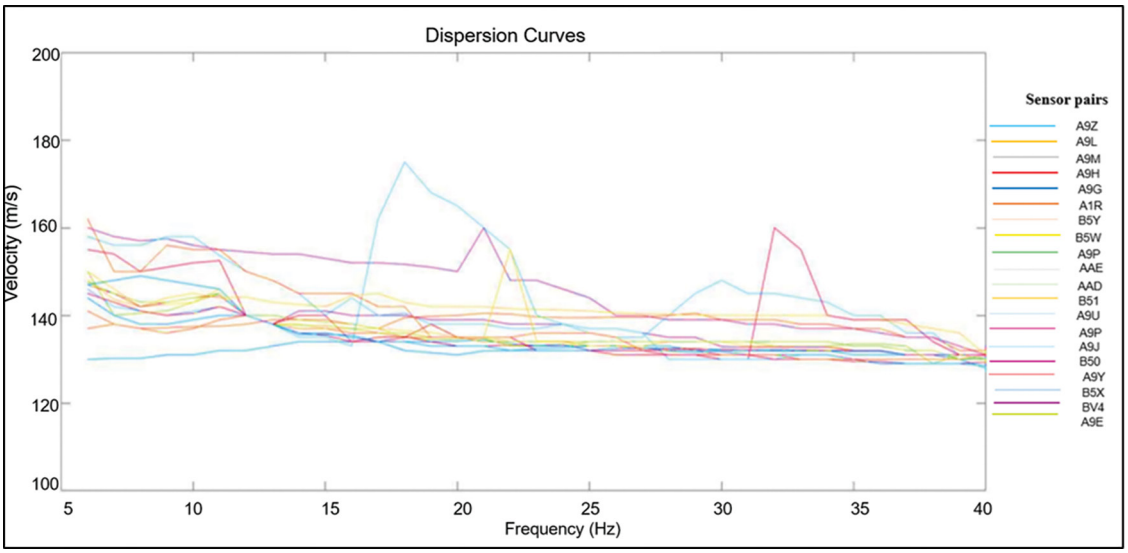

Figure 7: Diagram of the computed dispersion curves (phase velocity plotted against frequency). The plotted lines represent the average dispersion curve for the different sensor pairs.

We employed a Fast Fourier transform to shift the data into the frequency domain, which included phase-shifting the cross-correlation functions. We determined the relative energy for a particular frequency to obtain the slant-stacked amplitude for each set of virtual pairs. The technique included conducting a slant stack of filtered noise cross-correlation traces to create an image in the period-velocity domain. We filtered the traces and stacked them across various velocities at a particular frequency. The stack's amplitude enhances the correct velocity while suppressing others that do not align coherently. We then plotted the summed amplitude in the frequency domain to generate the dispersion curves.[25]

To determine the shear-wave velocity profile with depth, an improved neighbourhood algorithm described by Wathelet[26] was employed to invert the dispersion curves. The velocity changes with depth in the following manner: from the surface down to a depth of 4 m, the velocity spans a range of 240–164 m/s; between 4 m and 14 m, the velocity maintains a constant value of 164 m/s and then decreases to 158 m/s at a depth of 15 m (Figure 8). This decrease in velocity could result from increased saturation in this part of the dam wall.

The inversion analyses were conducted using the Dinver module within the open-source software Geopsy explained by Wathelet[26]. Shear wave velocities generally exhibit low values, with none surpassing 250 m/s at shallow depths between 1 m and 3 m. The average shear wave velocity at a depth of 20 m is 120 m/s. The presence of high velocity anomalies in the theoretical dispersion curve may stem from pre-existing anomalies in the data, which were incorporated into the inversion for analysis.

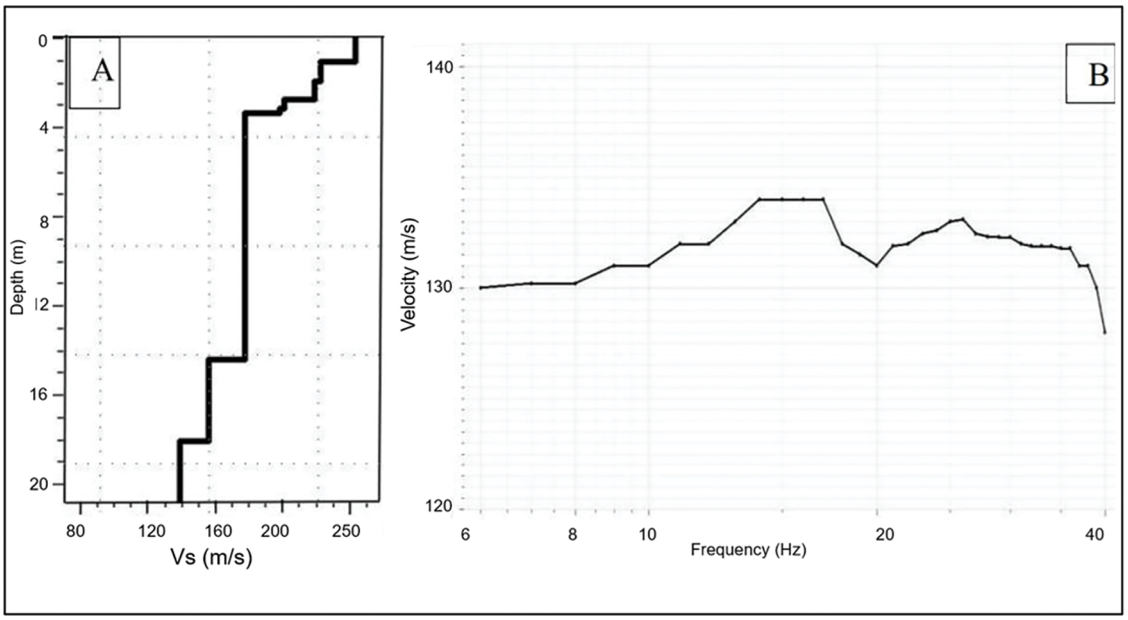

Figure 8: (A) 1D inverted profile and (B) theoretical dispersion curve that corresponds to the velocity model.

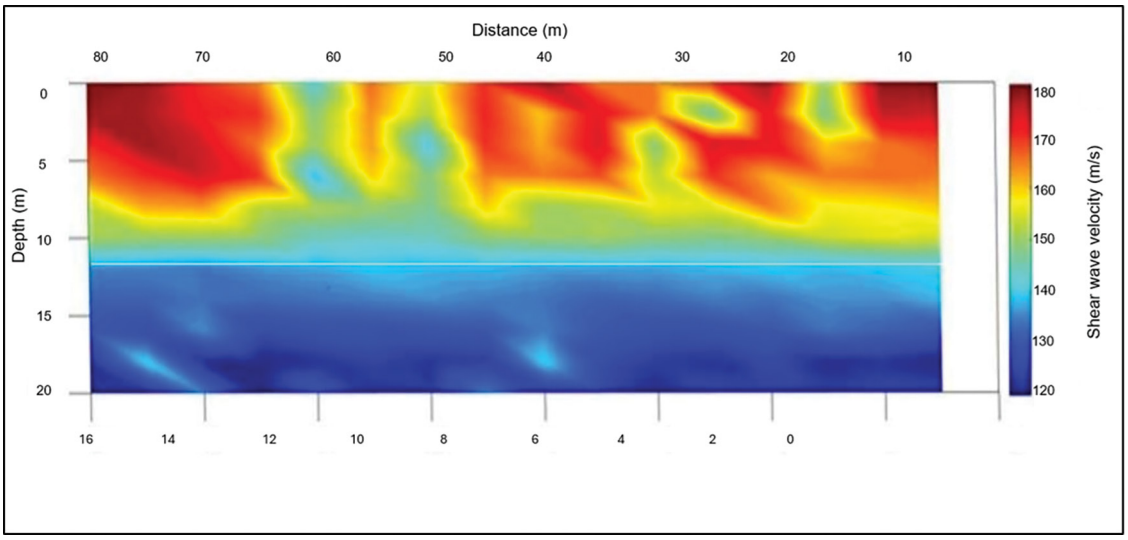

Figure 9: Cross-section of the shear wave velocity profile over 85 m of the section. The phreatic surface is represented by the low-velocity zone underneath the white line. The numbers at the bottom of the figure indicate geophone positions. The profile shows increasing distance from the right to the left and was plotted in this way to be consistent with the order in which the stations were planted. The stations were planted from the left to the right on the tailing dam wall.

The S-wave ground profile indicates higher velocities in the shallow portion (0–9 m). Following the inversion of all 30 dispersion curves, we assigned the resulting S-wave velocity profiles to the centroid of the sensor group used for constructing the shear wave velocity cross-section.

The final phase of the data processing approach involves creating a psuedo 2D shear wave velocity profile to generate a cross-section of surface and depth shear-wave velocities (Vs) (Figure 9). This is achieved by inverting all dispersion curves and implementing a bilinear interpolation method to create a 2D velocity grid data set. Subsequently, we utilised this data set to create a cross-section where different colour codes represent varying velocities.

Bilinear interpolation, a 2D interpolation technique, interpolates values along one axis and then along the perpendicular axis. It extends linear interpolation and is applied to interpolate functions with two variables on a rectangular 2D grid.

The horizontal resolution of the map is influenced by two field variables: the length of the receiver spread and the acquisition period. The virtual source spread length establishes the theoretical lower limit for spatial resolution, and any lateral dimension of a Vs structure smaller than this will not receive accurate resolution in the resulting Vs map. Spatial resolution can also be affected by processing accuracy, as each 1D Vs profile may contain errors arising from inaccuracies in the dispersion-inversion procedure's analysis.

Since the accuracy of stacking velocity significantly impacts the quality of seismic images, we employed interpolation to provide a more precise estimation of the stacking velocity. The initial step in determining stacking velocity involves interpolating time between picks at velocity analysis points. The subsequent step entails spatial interpolation to estimate stacking velocities at positions between the known velocity analysis points.

The upper layers at depths of 0 to 5 m display lateral variations in S-wave velocity, likely attributable to differences in soil compaction. Higher-velocity values may be associated with dense sand, while lower-velocity values may result from loose sand or soft clay.

A low-velocity zone that is close to the surface is detectable at 30 m, 50 m and 60 m along the profile, suggesting the possible presence of very loose sand or very soft clay in this region. Additionally, the S-wave profile shows a distinct low-velocity zone situated approximately 10 m below the surface. Two plumes with lower velocities ranging from 133 m/s to 140 m/s are observed between 50 m and 65 m near the array's core. This observation may indicate that the phreatic surface lies closer to the ground's surface.

Between distances of 70 m and 80 m, a high-velocity zone is discernible on the profile, suggesting the possible existence of dense sand. It is worth noting that the survey line closely corresponds to the area where the photograph providing evidence of seepage was taken (Figure 10).

Conclusion

Tailings dams play a critical role in storing mining waste, but they come with the inherent risk of failure, which can lead to severe environmental and human consequences. Traditional methods for assessing dam stability are resource-intensive and expensive, often relying on borehole drilling and physical measurements. Surprisingly, seismic methods, which offer continuous imaging of dam interiors, are underutilised in this context.

There is an urgent need for research and the development of innovative monitoring methods to track the evolving behaviour of these structures over time. Recent advancements in seismic interferometry have provided a way to use ambient noise to create virtual seismic sources at sensor locations, offering a cost-effective solution for monitoring subtle subsurface changes within tailings dams using standard passive micro-seismic monitoring equipment.

Our study aimed to employ ambient seismic noise to image the internal structure of a section of a tailings dam experiencing increased seepage. To accomplish this, we performed cross-correlation on seismic noise recorded from horizontal transverse geophone components, allowing us to estimate Love wave virtual source signals across the sensor array. We generated dispersion curves between different sensor pairs using these virtual source signals. To obtain 1D shear wave velocity profiles, we applied an improved neighbourhood algorithm to invert the dispersion curves.

Furthermore, we utilised virtual source signals to create dispersion curves between sensor pairs and employed the improved neighbourhood algorithm to invert these curves, resulting in 1D shear wave velocity profiles. We interpolated the profiles to construct a 2D shear wave cross-section along the survey line.

The resulting cross-section revealed a low-velocity zone approximately 12 m below the surface. Intriguingly, it also detected similar low-velocity zones at depths of 15, 50 and 60 m along the array, all positioned between 2 m and 10 m below the surface. These findings strongly suggest that the phreatic surface is notably closer to the surface in this specific region.

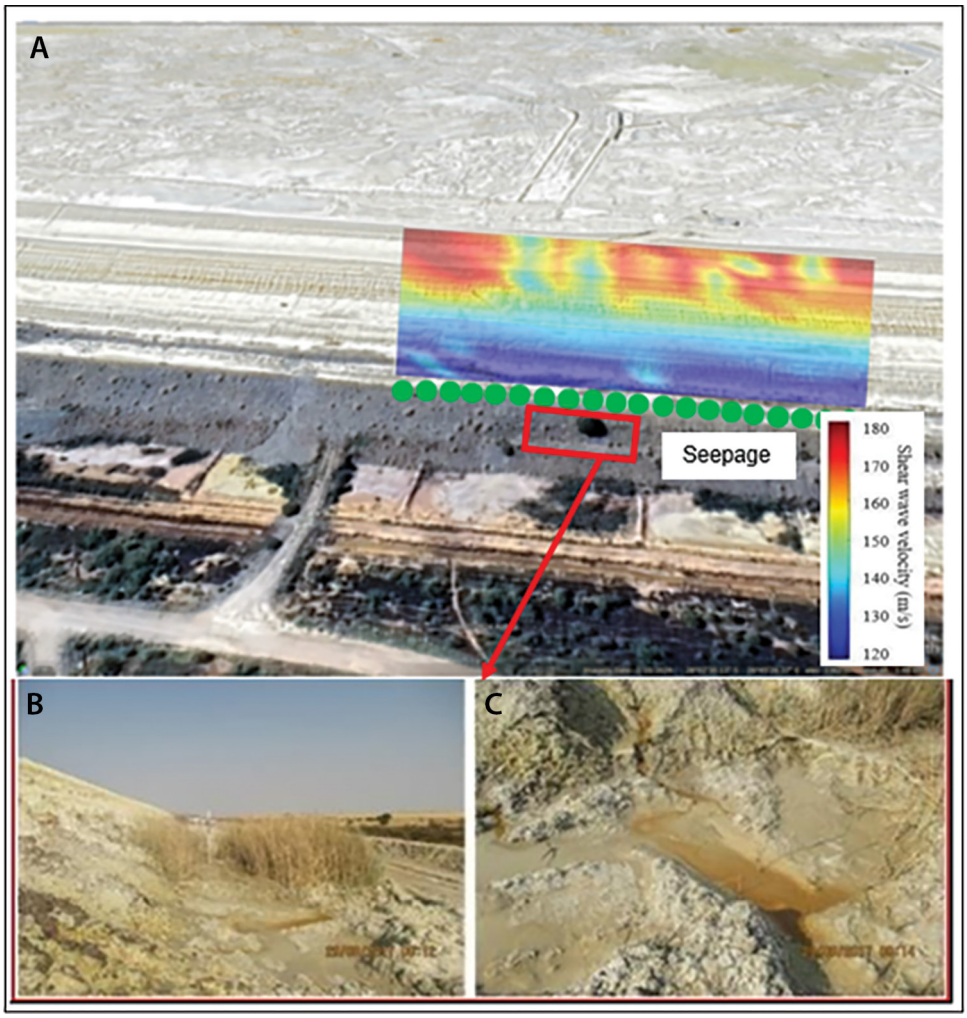

Source: (A) Google Earth.

Figure 10: The cross-section of the shear wave velocity profile overlain on the aerial image of the tailings dam to correlate with where the stations were deployed. (B) and (C) Pictures that were taken at the foot of the tailings dam. The images show indications of visible surface water and increased plant growth at the dam's base.

In summary, our study showcases the considerable potential of ambient noise tomography as a powerful tool for monitoring the structural integrity of tailings dams. By providing detailed subsurface images, this approach has the potential to identify potential risks and ultimately enhance the safety of these critical structures.

Funding

AEON provided financial support through its NRF-funded Iphakade programme.

Data availability

The data supporting the results of this study are available upon request to the corresponding author.

Acknowledgements

We thank Dr Lucian Bezuidenhout for his invaluable help with the seismic deployment and Dr Gerrit Olivier for assisting with a guide for the processing workflow.

Declarations

We have no competing interests to declare. We have no AI or LLM use to declare.

Authors' contributions

T.K.: Methodology, data collection, data analysis, data curation, writing – the initial draft. M.D.: Conceptualisation, writing – revisions, student supervision, project leadership, funding acquisition. Both authors read and approved the final manuscript.

References

1. Wang X, Zhan H, Wang J, Li P. The stability of tailings dams under dry-wet cycles: A case study in Luonan, China. Water. 2018;10(8):1–11. https://doi.org/10.3390/w10081048
2. Davies MP, Martin PE. Upstream constructed tailings dams – A review of the basics. In: Proceedings of the Tailings and Mine Waste. Boca Raton, FL: CRC Press; 2000. p. 3–15. https://doi.org/10.1201/9781003078579-2
3. Karombo T. South Africa has the world's highest number of environmentally dangerous tailing dams [webpage on the Internet]. c2020 [cited 2023 Mar 20]. Available from: https://qz.com/africa/1786297/south-africa-has-most-environmentally-dangerous-tailingdams
4. Stark TD, Moya L, Lin J. Rates and causes of tailings dam failures. Advances in Civil Eng. 2022;2022:1–21. https://doi.org/10.1155/2022/7895880
5. Minerals Council of South Africa. Merriespruit, 22 February 1994 [webpage on the Internet]. c2023 [cited 2024 Jul 02]. Available from: https://www.mineralscouncil.org.za/industry-news/we-care-we-remember/324-we-remember-merriespruit
6. Carnie T. River turns black after coal mine dam collapse next to rural communities and Hluhluwe-iMfolozi game reserve. Daily Maverick. 2022 January 11. Available from: https://www.dailymaverick.co.za/article/2022-01-11-river-turns-black-after-coal-mine-dam-collapse-next-to-rural-communities-and-hluhluwe-imfolozi-game-reserve/
7. Hansen K. South African town covered in mining waste after dam collapse. SciTechDaily. 2022 October 23. Available from: https://scitechdaily.com/south-african-town-covered-in-mining-waste-after-dam-collapse/
8. Njilo N. Free State mine dam burst floods kill three; four people critically injured. Daily Maverick. 2022 September 12. Available from: https://www.dailymaverick.co.za/article/2022-09-12-free-state-mine-dam-burst-floods-kill-three-four-people-critically-injured/
9. Clarkson L, Williams D, Seppälä J. Real-time monitoring of tailings dams. Georisk: Assess Manag Risk Eng Syst Geohazards. 2021;15(2):113–127. https://doi.org/10.1080/17499518.2020.1740280
10. Cheng F, Xia J, Xu Y, Xu Z, Pan Y. A new passive seismic method based on seismic interferometry and multichannel analysis of surface waves. J Appl Geophys. 2015;117:126–135. https://doi.org/10.1016/j.jappgeo.2015.04.005
11. Yang Y, Ritzwoller M. Characteristics of ambient seismic noise as a source for surface wave tomography. Geochem Geophys Geosyst. 2008;9(2):1–18. https://doi.org/10.1029/2007GC001814
12. Mao S, Lecointre A, van der Hilst RD, Campillo M. Space-time monitoring of groundwater fluctuations with passive seismic interferometry. Nat Commun. 2022;13:1–9. https://doi.org/10.1038/s41467-022-32194-3
13. Clements T, Denolle M. Tracking groundwater levels using the ambient seismic field. Geophys Res Lett. 2018;45(13):1–11. https://doi.org/10.1029/2018GL077706
14. Lehujeur M, Vergne J, Schmittbuhl J, Zigone D, Le Chenadec A. Reservoir imaging using ambient noise correlation from a dense seismic network. J Geophys Res Solid Earth. 2018;123(8):6671–6686. https://doi.org/10.1029/2018JB015440
15. Picozzi M, Parolai S, Bindi D, Strollo A. Characterization of shallow geology by high frequency seismic noise tomography. Geophys J Int. 2009;176(1):164–174. https://doi.org/10.1111/j.1365-246X.2008.03966.x
16. Draganov D, Wapenaar K, Thorbecke J. Seismic interferometry: Reconstructing the earth's reflection response. Geophysics. 2006;71:SI61–SI70. https://doi.org/10.1190/1.2209947
17. Carcione JM, Hans HB. Rock physics of geopressure and prediction of abnormal pore fluid pressure using seismic data. CSEG Recorder. 2002;27:9–32.
18. Bensen GD, Ritzwoller MH, Barmin MP, Levshin AL, Lin F, Moschetti MP, et al. Processing seismic ambient noise data to obtain reliable broad-band surface wave dispersion measurements. Geophys J Int. 2007;169(3):1239–1260. https://doi.org/10.1111/j.1365-246X.2007.03374.x
19. Xu Y, Koper KD, Burlacu R. Lakes as a source of short-period (0.5-2 s) microseisms: Microseisms from lakes. J Geophys Res Solid Earth. 2017;122:1–16. https://agupubs.onlinelibrary.wiley.com/doi/10.1002/2017JB014808
20. McNamara D, Boaz R. Visualization of the seismic ambient noise spectrum. In: Nakata N, Gualtieri L, Fichtner A, editors. Seismic ambient noise. Cambridge: Cambridge University Press; 2019. p. 1–18. https://doi.org/10.1017/9781108264808.003
21. Li X, Xu Y, Xie C, Sun S. Global characteristics of ambient seismic noise. J Seismol. 2022;26:343–358. https://doi.org/10.1007/s10950-021-10071-8
22. Ivanov J, Park CB, Miller RD, Xia J. Modal separation before dispersion curve extraction by MASW method. In: Proceedings of the Symposium on the Application of Geophysics to Engineering and Environmental Problems; 2001 March 04–07; Denver, CO, USA. Utrecht: European Association of Geoscientists & Engineers; 2001. p. 1–11. https://doi.org/10.3997/2214-4609-pdb.192.SSM_3
23. Lin FC, Ritzwoller MH, Townend J, Bannister S, Savage MK. Ambient noise Rayleigh wave tomography of New Zealand. Geophys J Int. 2007;170(2), Art. #649666. https://doi.org/10.1111/j.1365-246X.2007.03414.x
24. Foti S, Hollender F, Garofalo F, Albarello D, Asten M, Bard PY, et al. Guidelines for the good practice of surface wave analysis: A product of the InterPACIFIC project. Bull Earthquake Eng. 2018;16:2367–2420. https://doi.org/10.1007/s10518-017-0206-7
25. Luo Y, Xia J, Miller RD, Xu Y, Liu J, Liu Q. Rayleigh-wave mode separation by high-resolution linear Radon transform. Geophys J Int. 2009;179(1):254–264. https://doi.org/10.1111/j.1365-246X.2009.04277.x
26. Wathelet M. An improved neighborhood algorithm: Parameter conditions and dynamic scaling. Geophys Res Lett. 2008;35(9), Art. #L09301. https://doi.org/10.1029/2008GL033256